Tuning high power impulse magnetron sputtering discharge and substrate bias conditions to reduce the intrinsic stress of TiN thin films

Felipe Cemin, Grégory Abadias, Tiberiu Minea, Daniel Lundin

Tuning high power impulse magnetron sputtering discharge and substrate bias conditions to reduce the intrinsic stress of TiN thin films

Felipe Cemin[a,b], Gregory Abadias[c], Tiberiu Minea[a], Daniel Lundin[a]

[a] Laboratoire de Physique des Gaz et des Plasmas (LPGP), Unité Mixte de Recherche 8578 CNRS, Université Paris-Sud, Université Paris-Saclay, 91405 Orsay, France

[b] Current affiliation: Instituto de Física 'Gleb Wataghin' (IFGW-DFA), Universidade Estadual de Campinas, 13083-970 Campinas, Brazil

[c] Institut Pprime, Département Physique et Mécanique des Matériaux, Unité Propre de Recherche 3346 CNRS, Université de Poitiers, 86962 Chasseneuil-Futuroscope, France

E-mail: fcemin@ifi.unicamp.br

Abstract

Ion bombardment during film growth usually induces high compressive stress in compound thin film materials, resulting in rupture and failure of coated tools used in tribological applications. Hence, intrinsic stress generated during film growth can drastically limit the industrial appeal of deposition technologies such as high power impulse magnetron sputtering (HiPIMS). This work investigates how to reduce high stress levels by tuning the HiPIMS discharge conditions and selecting the appropriate substrate bias configuration. The strategy is based on optimizing the process discharge parameters, leading to HiPIMS discharges containing fewer multiply charged energetic metal ions, which is combined with pulsed substrate bias synchronized to the HiPIMS pulse to control the chemical nature of the incident ions, *i.e.*, inert gas *vs.* metal ions. The study was performed during growth of TiN thin films, due to their relevance as a protective coating, and the intrinsic stress was measured *in situ* during film growth using the wafer curvature method and a multi-beam optical stress sensor. The results show that for standard HiPIMS discharges and biased substrates, the energetic metal ion bombardment results in very dense, compact microstructures, but highly stressed TiN films. On the other hand, when using the here proposed strategy mentioned above, the compressive stress was considerably reduced (by a factor 11) while retaining rather compact microstructures compared to direct current magnetron sputtered as well as non-biased HiPIMS samples.

Keywords: high power impulse magnetron sputtering; substrate bias synchronization; intrinsic stress; titanium nitride; thin films

1. Introduction

High-power impulse magnetron sputtering (HiPIMS) is a promising deposition technique to synthesize thin and ultrathin films with significantly improved properties due to a high fraction of ionization of the sputtered species [1,2]. Optimization of the amount, direction, and energy of these ions during film growth has resulted in very smooth and dense films [3,4], control over their phase composition and microstructure [5,6], as well as enhanced mechanical [7] and electrical [8,9] properties. The use of HiPIMS has also been reported to be beneficial in terms of improving film adhesion [10], enabling deposition of uniform films on complex-shaped substrates [11,12], tailor the texture to grow epitaxial films even without substrate pretreatment [13], and achieving good film quality at a decreased deposition temperature [5,6,14].

However, ion bombardment during film growth also presents some challenges in that the impinging film-forming species typically have kinetic energies well above the thermal energy, which commonly induces high compressive stress by atomic-peening, defect generation, and/or grain boundary densification, in competition with stress relaxation by local heating in thermal spikes [15,16,17,18,19]. For example, Hovsepian *et al.* [20] report residual stress values for HiPIMS-deposited TiN films (~ 1 µm thick) of up to –11.7 GPa. Also Machunze *et al.* [21] report high compressive stress values of around –4 to –5 GPa for the same material system (film thickness < 150 nm) when using HiPIMS. In both cases, a direct current (DC) bias was applied to the substrate to tune the energy of the bombarding ionic species. Such high residual compressive stress values will likely result in rupture and failure of the TiN coating on cutting tools, drill bits, *etc.*

Greczynski *et al.* [22] tried to alleviate the problem by probing the effect of metal- *versus* rare gas-ion bombardment during $Ti_{1-x}Al_xN$ film growth using synchronized pulsed substrate bias in a hybrid HiPIMS/direct current magnetron sputtering (DCMS) configuration. When the

Al target was operated in HiPIMS mode and the Ti target in DCMS mode, they demonstrate that synchronizing the pulsed substrate bias in the time domain with the metal ion-rich (Al^+) portion of the HiPIMS pulse provides film densification, microstructure enhancement, surface smoothening, and no measurable Ar incorporation. More importantly for the present work, they managed to reduce the compressive stress of the film from –4.6 GPa when using DC bias to –0.9 GPa when using synchronized pulsed bias. However, the same strategy did not yield a significant reduction in film stress when the Ti target was operated in HiPIMS mode and the Al target in DCMS mode. In this case, they observed high compressive stresses, up to –3.5 GPa, which the authors ascribed to a large fraction of Ti^{2+} ions in the material flux [23]. These doubly charged ions increase the average metal-ion momentum per deposited atom and generate significant residual ion damage leading to high concentrations of point defects, which give rise to the observed high compressive stress [23]. These results show that stress tailoring is still an issue in HiPIMS when sputtering elements which are easily ionized to charge states $q \geq 2$. This is, for example, the case for Ti and Nb [24,25], where the second ionization potentials ($\phi_{\mathrm{iz,Ti}}^{1\rightarrow 2} = 13.58$ eV and $\phi_{\mathrm{iz,Nb}}^{1\rightarrow 2} = 14.32$ eV, respectively) are lower than the first ionization potential for the process gas (typically Ar with $\phi_{\mathrm{iz,Ar}}^{0\rightarrow 1} = 15.76$ eV), which leads to high fractions of doubly charged metal ions [26] (strictly speaking, one should compare the electron impact cross-sections for the relevant ionizing reactions, although the ionization potential serves as a good enough indicator when estimating high or low ionization).

To overcome this issue, we here investigate the possibility of tuning the pulse and process conditions in reactive HiPIMS of a Ti target, for reducing the amount of multiply charged ions of the sputtered species in combination with the above-described use of synchronized substrate bias to ultimately minimize the compressive intrinsic stress of TiN films. TiN was chosen as a suitable material system not only due to its potential to provide multiply charged ions but also due to its relevance as a protective coating, *e.g.*, in high-speed steel cutting tools and drill bits, where high hardness and high wear resistance [27,28] are required. The performance and lifetime

of these materials are directly related to the stress levels acquired during film growth. Other typical areas of use for TiN include diffusion barriers, anti-reflective layers, adhesion-promoting layers in semiconductor devices, decorative layers in jewelry, eyeglasses and cutlery [28,29,30], biocompatible overlayers [31], as well as a potential material for plasmonics [32,33,34].

The film stress magnitude and stress evolution with thickness were evaluated by *in situ* wafer-curvature measurements during film growth, which corresponds exclusively to the stress generated by the processes involved in the deposition, and is therefore referred to as the "intrinsic stress" [35]. A large set of process conditions were scanned in order to identify the best operating point. These choices were guided by the results of Ross *et al.* [36], who showed that high peak current densities $J_{D,peak}$ in HiPIMS favor the formation of multiply charged Ti ions (*e.g.*, Ti^{2+}) at the expense of singly charged ions (Ti^{+}) as well as by Kubart *et al.* [37] and Lundin *et al.* [38], who investigated how the ionized flux fraction of Ti changes with $J_{D,peak}$.

2. Experimental Details

The studied TiN films were deposited by HiPIMS (and DCMS in one specific reference case) onto Si(001) oriented wafers, 199 ± 4 µm thick, covered with a native oxide (SiO_x) layer, without any prior substrate cleaning process. The depositions were carried out in a high-vacuum chamber (base pressure $< 10^{-5}$ Pa) equipped with a bottom-mounted, 7.5 cm-diameter high purity (99.995 %) Ti target operated by either a HiPIMS power supply (HiPSTER 1, Ionautics, Sweden) or a DC power supply (SR1.5-N-1500, Technix, France). Ar was used as the working gas and N_2 as the reactive gas (both 99.9999 % purity). The target was located at 18 cm from the top-mounted substrate holder, which was coupled to a resistive element for sample heating. All samples were deposited at the same substrate temperature (300 °C), target average power (300 W), and N_2 gas partial pressure ($7.4 \pm 0.5 \times 10^{-3}$ Pa). In order to provide suitable HiPIMS discharge conditions in terms of ionization and energy of the ionic species (before applying a substrate bias), the target peak current during the pulse ($I_{D,peak}$) and the total gas pressure (p)

were both modified to ensure two types of HiPIMS discharges with rather different characteristics. The reason for varying these two parameters is that the amplitude of $I_{\mathrm{D,peak}}$ is well-known to influence the ionized flux fraction as well as the fraction of multiply charged Ti ions, as already discussed in the introduction and widely demonstrated for different experimental setups [36,37,38]. Here, a higher $I_{\mathrm{D,peak}}$ increases the fraction of multiply charged ions [25,36]. On the other hand, the choice of total gas pressure will affect the particle energy, where a higher p leads to a lower kinetic energy of the metal ions, due to more collisions with Ar gas atoms during transport to the substrate [39].

Therefore, in the first investigated discharge type, hereon referred to as "Moderate-energy HiPIMS", a fairly standard HiPIMS discharge was obtained, by applying $I_{\mathrm{D,peak}} = 16.4$ A to the target (equivalent to a peak current density of $J_{\mathrm{D,peak}} = 0.36$ A cm^{-2}) and using a total gas pressure of $p = 0.37$ Pa (Ar gas flow rate = 57 sccm and N_2 gas flow rate = 0.5 sccm). Square voltage pulses of –570 V with 100 µs pulse-on time and a pulse frequency of 400 Hz (duty cycle of 4 %) were applied to the target. For comparison, a single DCMS TiN sample was also deposited using the same p value. For the second discharge type, referred to as "Low-energy HiPIMS", a discharge containing less energetic species was obtained by using only $I_{\mathrm{D,peak}} = 8.8$ A (or $J_{\mathrm{D,peak}} = 0.19$ A cm^{-2}), while operating at almost twice the total gas pressure used before, *i.e.*, $p = 0.60$ Pa (Ar gas flow rate = 108.5 sccm and N_2 gas flow rate = 0.85 sccm). In order to keep the same target average power, the voltage was decreased to –460 V and the pulse frequency was increased to 950 Hz, which resulted in a duty cycle of 9 %. Typical voltage and current waveforms used in the Low-energy HiPIMS discharges are shown in Fig. 1a.

Each batch of samples deposited using Moderate- and Low-energy HiPIMS discharges, was exposed to the following set of substrate conditions: (1) electrically grounded (0 V), (2) polarized to –60 V using a DC bias power supply (SR1-N-300, Technix, France), or (3) synchronized pulsed bias at –60 V using a custom-built pulsed bias unit coupled to a

synchronization unit (HiBi & HiPSTER Sync Unit, Ionautics, Sweden), where the latter device is capable of synchronizing both the pulsed bias unit and the HiPIMS unit. For synchronized biasing, a bias pulse width of 100 µs was selected and activated at different delay times ($t_{\mathrm{bias}} =$ 1, 30, and 60 µs) with respect to the HiPIMS discharge pulse, and repeated at a common frequency, which was equal to 400 Hz for the Moderate-energy series and 950 Hz for the Low-energy series. The choice of delay times are related to the estimated arrival-times of the metal ions, which is discussed in more detail in the Section 4. The different substrate conditions described here are represented in Fig. 1b-e through their bias voltage waveforms captured during the experiments. Please note that the non-zero bias value observed in the beginning of the bias voltage waveforms in Fig. 1c-e before activating the pulsed substrate bias is due to the floating potential on the substrate holder. Moreover, all pulsed bias waveforms show a slope at the end of the pulse, which is due to slow discharging of the capacitors in the absence of a dense plasma.

The intrinsic stress evolution was determined *in situ*, in real time, by wafer curvature measurements during growth of all studied TiN films, 200–400 nm thick, using a multi-beam optical stress sensor (MOSS) designed by k-Space Associates (*k*SA), Inc, USA, and installed in the sputtering system, with a curvature resolution of 2×10^{-4} m^{-1}. It is composed of a 2D array of parallel laser beams created by highly reflective X and Y etalons and recorded on a high-resolution charge-coupled device (CCD) camera with a typical acquisition rate of 2 Hz. A schematic illustration of the experiment set-up is shown elsewhere [40]. The measured wafer curvature $\Delta\kappa$ is proportional to the product between the average stress $\langle\sigma\rangle$ and film thickness h (also named film force per unit width, F/w) [35,41], through the modified Stoney equation $\frac{F}{w} = \langle\sigma\rangle\ h = \frac{1}{6} Y_s\ h_s^2\ \Delta\kappa$ [42], where h_s is the substrate thickness and Y_s is the biaxial modulus of the substrate, which was assumed to be equal to 180.5 GPa for (001) single crystal Si wafers [43]. $\langle\sigma\rangle$ is obtained by dividing F/w with the film thickness at each point. By convention, positive $\langle\sigma\rangle$ values refer to a tensile stress state, while negative values correspond to a compressive stress state.

The chemical composition of the films was measured by electron probe microanalysis using a JEOL 7001 TTLS scanning electron microscope (SEM) equipped with a wavelength X-ray dispersive spectroscopy (WDS) unit from Oxford Instrument. The acceleration voltage was set at 10 kV and the beam current fixed at 20 nA. The film thickness, density and roughness were determined by X-ray reflectometry (XRR) using a Seifert XRD3000 diffractometer in parallel beam configuration, for TiN films < 80 nm thick deposited under the same experimental conditions as those used for wafer curvature measurements. SEM was performed on the thicker TiN films (200–400 nm) by analyzing their cross-sections, in order to confirm the thickness values predicted by XRR, using an ultra-high resolution field-emission FE-SEM Hitachi SU8000. The crystallographic orientation of the same samples was determined by X-ray diffraction (XRD) in conventional θ–2θ scans carried out on a Seifert XRD TS-4 diffractometer operating in the Bragg-Brentano configuration at $\lambda = 0.15418$ nm wavelength and equipped with a Meteor0D detector. The room temperature (RT) electrical resistivity, ρ_{el}, was measured under Van der Pauw geometry using an Ecopia HMS-5500 system.

3. Results

3.1. Intrinsic stress

This section presents the results on the intrinsic stress of the studied TiN films, obtained from *in situ* wafer curvature measurements during film growth. The evolution of the film force (F/w) with film thickness in Moderate- and Low-energy HiPIMS modes is shown in Fig. 2a and 2b, respectively, when using the different substrate conditions described in the Experimental Details. For the films deposited by Moderate-energy HiPIMS (Fig. 2a), F/w decreases monotonically with thickness when biasing the substrates, independently of the bias configuration (DC or synchronized pulsed at different delay times). However, when the substrate is grounded, F/w decreases much more slowly and is nearly constant for a film thicknesses $>$ 100 nm. Fig. 2a (dashed line) also shows the film force evolution for a TiN sample deposited by

DCMS at the same total gas pressure and average target power, on a DC biased substrate. In this specific case, F/w is nearly constant, and slightly positive, independently on the film thickness. The corresponding results for the Low-energy HiPIMS series are presented in Fig. 2b. The DC biased sample exhibits the most negative film force of all investigated samples, whereas the pulsed biased samples show a much lower decrease of F/w followed by steady-state regimes for film thicknesses > 100 nm. The grounded sample shows slightly positive film forces, and no DCMS sample was investigated for the Low-energy conditions.

The average intrinsic stress curves for the same samples are presented in Fig. 2c and 2d, for both Moderate- and Low-energy HiPIMS discharges, respectively. In the Moderate-energy series (Fig. 2c), the intrinsic stress is highly compressive for the HiPIMS samples deposited on either DC or pulsed biased substrates, with average stress values around –11 GPa in the steady-state regime, *i.e.*, when the stress is constant with film thickness. Only small changes are observed when using different delay times in pulsed biased substrates, and the sample deposited at $t_{\mathrm{bias}} = 60$ µs shows the highest compressive stress. However, one notices that the grounded sample shows much lower compressive stress and it evolves with film thickness, to reach a steady-state regime at thicknesses > 200 nm (not investigated). The DCMS TiN film shows a tensile stress, but is very close to zero. From the average intrinsic stress curves for the Low-Energy HiPIMS series, shown in Fig. 2d, it is seen that the highest compressive stress was obtained using a DC biased substrate. This is not surprising considering the evolution of the corresponding F/w curves in Fig. 2b. The average stress evolves with film thickness, being equal to –5.2 GPa at 200 nm. The use of a pulsed substrate bias synchronized with the HiPIMS discharge pulse reduces significantly the compressive stress, as observed in Fig. 2d, to nearly-steady-state values of –1 GPa (or less) at the same film thickness of 200 nm. As observed before, the sample deposited at $t_{\mathrm{bias}} = 60$ µs shows the highest compressive stress among the pulsed biased samples. Finally, the grounded sample showed a very low tensile stress of +0.1 GPa.

In order to simplify the comparison, Fig. 3 shows the average stress values of all films investigated in Fig. 2, as a function of the substrate condition (grounded, DC or synchronized pulsed biased at different delay times). One notices that the HiPIMS discharge conditions (Moderate- or Low-energy) as well as the different substrate bias configurations have a strong influence on the intrinsic stress of TiN films deposited. It is important to note that most of these values are referring to film growth conditions where the average stress no longer change with film thickness, *i.e.*, at the steady-state regime. Indeed, for the Moderate-energy HiPIMS series (blue circles), the values at 100 nm film thickness were selected, since the intrinsic stress is found constant (Fig. 2c) and is assumed to remain constant for higher thicknesses. The only exception concerns the grounded sample, with the average stress evolving from –1.9 GPa at 100 nm to –0.9 GPa at 200 nm (Fig. 3 shows the value at 100 nm). For the Low-energy series (red squares), we chose a film thickness of 200 nm, because a steady-state regime was not completely established at 100 nm for most samples, see Fig. 2d.

3.2. Microstructure

The XRD patterns of selected TiN films investigated above are shown in Fig. 4a and Fig. 4b over the angular range between 32 to 65° using the Moderate-energy and the Low-energy discharges, respectively. All patterns exhibit characteristic diffraction peaks corresponding to polycrystalline TiN with cubic (NaCl-type) structure, according to the JCPDS card no. 38-1420. For the films deposited by Moderate-energy HiPIMS (Fig. 4a), only 111 and 200 XRD lines are detected in the investigated angular range, with texture coefficients (T_c) [44] equal to ~1.6 and ~0.4, respectively. The T_c values do not considerably change for the different investigated samples (see Table 1), indicating a (111) preferred orientation independently on the substrate condition during film growth. However, when biased substrates are used, the 111 XRD line is shifted towards lower angle by approximately 0.24° from its expected 2θ position. This shift is consistent with the compressive residual stress state of these films, as determined from the *in situ* wafer curvature measurements presented earlier. However, one can notice that the peak shift is

less pronounced for the 200 XRD line. Lattice parameters extracted from the 111 and 200 peak positions yield a_{111}= 0.4292 and a_{200}= 0.4255 nm, respectively. Similar trends in peak shift, and associated lattice expansion, were reported by Pelleg *et al.* [45] and Petrov *et al.* [46] in TiN films deposited by DCMS. The observed difference in lattice parameter cannot be explained solely by anisotropy in the elastic constants [47], suggesting also different ion-irradiation induced residual defect densities depending on crystallite orientations. Analysis of the XRD line broadening using the Scherrer formula [48] shows that the average size of crystallites oriented with their [111] direction normal to the substrate is larger than that of crystallites oriented along the [200] direction, and decreases from 22 nm (grounded sample) to 14 nm (biased samples) in the case of crystallites preferably oriented along the [111] direction.

For the films deposited by Low-energy HiPIMS (Fig. 4b), the XRD patterns show the typical 111 and 200 lines as well as an additional 220 XRD line. The grounded sample corresponds to a polycrystalline TiN film with random orientation, as $T_c \cong 1$ for all identified diffraction peaks. The DC biased sample tends to develop a (100) preferred orientation, with $T_{c\,(200)} = 1.4$. In addition, one notices that the XRD peaks are slightly shifted towards lower angles with respect to positions for bulk reference powder, in agreement with the larger compressive stress state found for this sample. Finally, the pulsed biased samples exhibit a stronger (100) texture, with $T_{c\,(200)} = 2.1$. Although we only show in Fig. 4b the XRD data for the pulsed biased sample with synchronization at $t_{\mathrm{bias}} = 60$ µs, a similar behavior was observed for the samples with synchronization at $t_{\mathrm{bias}} = 1$ µs and 30 µs (see Table 1). Using the Scherrer formula, we found a typical [200] crystallite size of ~30 nm for the grounded and pulsed biased samples, and 19 nm for the DC biased sample, *i.e.*, somewhat larger compared to the Moderate-energy series.

Cross-sectional SEM images of selected TiN films are shown in Fig. 5. The microstructure differs for the different samples, which were deposited using Moderate-energy (a-b), DCMS (c), and Low-energy discharges (d-f). For Moderate-energy HiPIMS, the use of a pulsed bias synchronized to the HiPIMS pulse ($t_{\mathrm{bias}} = 1$ µs, Fig. 5b) resulted in a much more compact

microstructure of the thin film, with a smother top-surface, compared to the HiPIMS film deposited on a grounded substrate (Fig. 5a). This is confirmed by quantitative XRR analysis, which shows that pulsed-biased films are exceptionally dense, with a mass density equal or even slightly higher than the bulk value of 5.4 g cm^{-3} [28], whereas the density of the grounded film is 5.2 g cm^{-3}. The results are summarized in Table 1. On the other hand, the TiN film deposited by DCMS using a DC biased substrate, at the same average power and total gas pressure (Fig. 5c), showed a fibrous, under-dense, columnar structure, with a rough, facetted top surface typically reported for polycrystalline TiN films growing with competitive (111) preferred orientation [49]. The film density, extracted from XRR, is 4.55 g cm^{-3}, which is ~16% lower compared to the bulk value and the pulsed bias HiPIMS samples deposited at the same total gas pressure. For this sample, the surface roughness determined from XRR is 7.2 nm, which is significantly higher than the values obtained for pulsed-bias HiPIMS TiN films (~1.3 nm), see Table 1.

SEM cross-sectional images are also presented for selected samples of the Low-energy series. Here, only TiN films (< 400 nm thick) deposited by HiPIMS are displayed, using grounded (Fig. 5d), pulsed biased (Fig. 5e) and DC biased (Fig. 5f) substrates. At first glance, these images show TiN films with a less compact microstructure compared to the TiN HiPIMS films of the Moderate-energy series (Fig. 5a,b), as also supported by the lower film density of this series which ranges from 4.15 (grounded) to 5.10 g cm^{-3} (DC bias). These films also develop a rougher surface compared to the Moderate-energy series, see Table 1. The use of a pulsed bias synchronized to the HiPIMS pulse (Fig. 5e) resulted in a more compact microstructure compared to the film deposited on a grounded substrate (Fig. 5d), as also observed in the Moderate-energy series. Finally, the TiN HiPIMS film deposited on a DC biased substrate showed the most compact structure of the Low-energy series, which is also consistent with the higher compressive stress of this sample (see Fig. 3).

The RT electrical resistivity has been measured for both Moderate- and Low-energy film series. Values are reported in Table 1. Low ρ_{el} values, around 30 μΩ cm, are found for the

pulsed-bias TiN HiPIMS films deposited under Moderate-energy conditions. These are among the lowest values reported for polycrystalline sputtered TiN films [50], approaching the resistivity values of single-crystal epitaxial TiN layers (12.4 μΩ cm [51], 18 μΩ cm [51,52]) or bulk TiN (~25 μΩ cm [51,52]). Higher ρ_{el} values around 90–130 μΩ cm are obtained for the Low-energy pulsed-biased film series, while a noticeable increase in electrical resistivity is observed for the films with the lowest density (grounded substrate condition at Low-energy and DCMS TiN films).

WDS analysis reveals that the chemical composition of the deposited TiN films does not vary with the investigated plasma discharge or substrate bias conditions. Films of both Moderate- and Low-energy series are slightly under-stoichiometric (N/Ti ~ 0.8), see Table 1. The oxygen content was also measured: for the densest films, a value of 2–3 % is measured, arising essentially from surface contamination and from the native silicon oxide of the Si substrate, while it increases up to 8 % and 14 % for the grounded and DCMS samples, respectively. This is consistent with the more open columnar microstructure and lower mass density of these samples, which favors oxygen uptake after deposition, and is also in line with their higher electrical resistivity values, see Table 1.

4. Discussion

Let us start by addressing the standard HiPIMS conditions, represented by the Moderate-energy series, since such deposition conditions are typically encountered within the existing HiPIMS literature. The very high intrinsic compressive stresses (–11 GPa) found for the TiN films deposited by Moderate-energy HiPIMS on (DC or pulsed) biased substrates are similar to the values found by Hovsepian *et al.* [20] for HiPIMS TiN films deposited at comparable experimental conditions (p = 0.3 Pa, T = 400 °C, –50 V DC bias). High compressive stress values were also reported for other refractory materials deposited by HiPIMS [53,54], which is not adequate for many applications.

The reason for such high compressive stresses is found in the very high flux fraction of energetic species reaching the substrate during film growth. Based on mass spectrometry measurements under similar conditions, we assume an average kinetic energy (E_{kin}) for Ti^+ and Ti^{2+} ions of 15–20 eV [55,56] with the Ti^{2+} population having a slightly higher E_{kin} than the Ti^+ population [23] and with energetic tails reaching up to about 100 eV [55] (the precise ion energy distributions are not that important for our discussion in contrast to the average values). In addition, few collisions with the working gas are expected in the plasma bulk at the chosen total pressure (p = 0.37 Pa), since the mean free path is $\gtrsim$ 5 cm (and increasing with increasing ion energy). When a bias voltage of –60 V is applied to the substrate the Ti^+ ions will be accelerated in the substrate sheath. The gained accelerating energy (E_{acc}) is very close to the bias value, *e.g.*, $E_{acc} \approx$ 60 eV, since a collisionless sheath is commonly assumed in these discharges. For Ti^{2+}, E_{acc} is twice the bias value, due to the charge state $q = 2$. Thus, the total energy ($E_T = E_{acc} + E_{kin}$) of the impinging ions in this situation is approximately $\gtrsim$ 80 eV for Ti^+ ions and $\gtrsim$ 140 eV for Ti^{2+} ions. In this context, we have to pay attention to the Ti^{2+} ions in particular, since they are likely to impinge onto the growing film with the highest energy. Increasing the ion energy significantly above the bulk lattice displacement threshold, $\gtrsim$ 20 eV depending on the material system (mass of the bombarding particle and layer composition) [57,58], will, at high enough E_T, significantly increase the defect density (incorporation of intragranular residual damage) so that renucleation leading to high compressive stress occurs [59,60]. For example, Patsalas *et al.* [61] reported that the subplantation energy threshold for TiN is 50 eV, providing an estimate of the energy required to incorporate defects in the layer by atomic peening processes. During growth of TiN by DCMS, Petrov et al. [59] show that for ion energies $E_T >$ 160–200 eV (mainly Ar^+ ions), local epitaxial growth on individual columns is disrupted leading to renucleation. Note that this is in the same energy range as the Ti^{2+} ions in the present case. Our results are also in line with the work of Greczynski *et al.* [23] on TiAlN, where they observe high compressive stresses, up to –3.5 GPa, when running the Ti cathode in the HiPIMS mode. The authors ascribe this to a

large fraction of Ti^{2+} ions in the material flux, as verified by mass spectrometry. Although absolute quantities cannot be determined using this technique, we can still get an idea of the amount of Ti^{2+} ions present in HiPIMS discharges from discharge modeling. Gudmundsson *et al.* [62] investigate fairly standard peak current densities around 0.5 A cm^{-2} at a total pressure of 0.6 Pa and find an ion density fraction of $n_{Ti^+}/n_{Ti^{2+}} \approx 20$ in the ionization region (~ magnetic trap). However, when increasing the peak current density to 1.6 A cm^{-2} they find that $n_{Ti^+}/n_{Ti^{2+}} \approx 4$. Significant amounts of Ti^{2+} ions are therefore expected in HiPIMS Ti discharges unless operating at considerably reduced peak currents.

In addition to the high compressive stress discussed above, these energetic ions may favor the formation of high-density structures due to higher adatom diffusivity, as evidenced by the cross-sectional SEM image of the Moderate-HiPIMS sample deposited using pulsed bias in Fig. 5b. All the pulsed biased samples of this series show a high density, close to the bulk value of TiN, a compact, void-free microstructure, and low resistivity (30 μm cm), see Table 1. A correlation between film density, intrinsic stress state and electrical resistivity was established. As an illustration, Fig. 6 displays the evolution of intrinsic stress *vs.* electrical resistivity for all investigated samples. Films with higher compressive stress exhibit the lowest ρ_{el} values. Our data are consistent with previous work by Patsalas et al. [63] who observed a correlation between hardness and resistivity when changing the bias voltage from –20 to –100 V, due to increasing mass density from 4.3 to 5.6 g cm^{-3}. It is also important to note that TiN film resistivity is strongly affected by chemical composition, as demonstrated by Shin *et al.* [64]. However, in the present case, the N/Ti ratio is the same for all studied samples (Table 1), *i.e.*, changes in resistivity depend mostly on film microstructure.

The grounded sample deposited in the Moderate-energy HiPIMS series showed much lower compressive stress (–0.9 GPa) compared to the previous case, as well as lower mass density and, therefore, higher electrical resistivity. For comparison, Hovsepian *et al.* [20] and Machunze *et al.* [21] obtained compressive stress values of –3 GPa and –0.5 GPa, respectively, for TiN films

deposited by HiPIMS on grounded substrates, using similar deposition conditions. This is mainly due to the fact that the total energy of the bombarding ions in this case is much lower, since $E_{acc} \approx 0$ eV, *i.e.*, $E_T \approx E_{kin} \approx$ 10–20 eV according to our discussion above, even in the case of Ti^{2+} ions. Thus, a significant part of the ion population has an energy which is below the bulk lattice displacement threshold. However, it should be pointed out that this sample still exhibits a relatively high mass density (5.20 g cm^{-3}). This is in line with the results by Lattemann et al [4], who used HiPIMS to deposit fully dense, non-faceted 111-textured TiN films without any external substrate heating or bias.

The DCMS TiN film deposited on a DC biased substrate showed a low tensile stress, equal to +0.1 GPa (Fig. 2c), associated with pronounced columnar microstructure (Fig. 5c) and reduced mass density (4.55 g cm^{-3}). The development of tensile stress is typical for films with underdense microstructure, and the result of attractive forces acting at the column boundaries [65,66]. This tensile stress state is correlated to a higher electrical resistivity (see Fig. 6). In DCMS discharges, Ti is mainly found as a neutral species, and the ionic flux reaching the substrate is dominated by Ar^+ ions [67,68,69], which is known to lead to detrimental residual ion-induced compressive stress due to Ar entrapment and generation of defects [15,70,71]. However, this is clearly not the case in the current situation, where the stress is close to zero. Instead, we believe that this is a result of the long target-to-substrate distance (0.18 m) in the present experiment, which effectively separates the dense plasma zone from the substrate region. Ionization of neutral Ar with a random velocity distribution will occur in the ionization region close to the target, but very few Ar^+ ions will reach the substrate due to a non-directional velocity. Such gas ions, with significantly lower E_{kin} compared to the Ti^+ and Ti^{2+} ions [72], will also undergo more collisions with the neutral working gas during transport, which will further limit the possibility of reaching the substrate. Note that this situation is very different from the sputtered species, with a velocity component directed mainly towards the substrate. Also remember that the Ar^+ ion density is at least two orders of magnitude lower in DCMS compared to in HiPIMS, due to the lower plasma

density, while the neutral flux is higher. It is therefore concluded that Ar^+ ion bombardment of the film surface during growth is limited in the DCMS case investigated here.

Of much more interest are the TiN samples deposited by Low-energy HiPIMS in combination with substrate biasing with considerably lower stress levels compared to the Moderate-energy series. The compressive stress is reduced from ~11 GPa (Moderate-energy series) to ~1 GPa (Low-energy series) when using pulsed substrate bias, *i.e.*, by a factor 11, see Fig. 3, while retaining rather compact microstructures (Fig. 5e, mass density ~4.8 g cm^{-3}) compared to the DCMS (Fig. 5c, mass density ~4.5 g cm^{-3}) as well as the non-biased sample (Fig. 5d, mass density ~4.1 g cm^{-3}). This huge difference in residual stress between the Low- and Moderate-energy series cannot be explained by the change in texture, as the elastic anisotropy for TiN is rather small (Zener anisotropy ratio of 1.36) [47].

The electrical resistivity of these samples is around 90–130 μΩ cm, which stands at the inflection point of the curve in Fig. 6, between the values of the Moderate-energy series (~30 μΩ cm) and the DCMS sample (~267 μΩ cm). These results show that thin film properties and structures can be improved, while considerably reducing their compressive stresses, by modifying the HiPIMS process towards the low-energy conditions and fine-tuning using the substrate bias. Moreover, these modified discharge conditions provide access to a new process window characterized by films with low to medium-low compressive stress, while retaining the beneficial HiPIMS film properties to a large degree. By looking at the stress-resistivity curve in Fig. 6, we find that this process window is situated between the standard HiPIMS discharge conditions represented by the Moderate-energy series and the DCMS process. This is explained as follows:

The chosen discharge conditions in the Low-energy series are expected to generate mainly Ti^+ ions, but significantly fewer Ti^{2+} ions by limiting the peak current, in line with observations reported by Ross *et al.* [36]. These ions undergo more collisions during transport to the substrate, due to the higher pressure (0.6 Pa) used for this series. As a consequence, E_{kin} is likely reduced

to approximately 5–10 eV, although precise values have not been established in this study. When using a bias voltage of –60 V, $E_{acc} \approx 60$ eV, the total amount of energy of the Ti^+ impinging ions is $\lesssim 70$ eV, *i.e.*, lower energies as compared to the Moderate-energy series. The much lower intrinsic stress values are also an additional indication of the absence of Ti^{2+} ions.

In the pulsed bias case, the compressive stress is seen to increase from –0.35 GPa to –0.95 GPa when the delay time of the pulsed bias is increased from 1 μs to 60 μs, see Fig. 2d. To understand this, let us analyze the plasma conditions. Most Ti ions that combine with nitrogen to form a TiN film on the sample surface are created in the ionization region close to the Ti target, on a time scale that typically corresponds to a few tens of μs after the beginning of each HiPIMS pulse [1,23,36]. Then, they are transported toward the substrate, *i.e.*, a distance of 0.18 m in our case, with an estimated flight time of ~30–40 μs, considering a Ti ion with an energy of 5–10 eV. Therefore, these ions will reach the substrate sheath around 60–80 μs after the onset of each 100 μs HiPIMS pulse. For a pulsed biased substrate with $t_{\mathrm{bias}} = 1$ μs, the bias pulse matches the HiPIMS pulse in the time domain, thus, very few Ti^+ ions are accelerated by the bias potential, since they arrive too late (during the last ~20 μs of the pulse). The energetic metal ion bombardment is thereby reduced, resulting in low compressive stress (–0.35 GPa). On the other hand, for a bias pulse delay time of 60 μs, most of the Ti^+ ions reaching the substrate sheath will be accelerated to the growing film by the bias potential, resulting in a more intense metal ion bombardment during film growth and thus, higher compressive stress (–0.95 GPa). An intermediary situation is found for the $t_{\mathrm{bias}} = 30$ μs case.

The grounded sample also showed a very low stress, but tensile, and equal to +0.1 GPa. As explained before for the Moderate-energy series, at grounded bias, the energy of the bombarding ions is much lower, and roughly equal to E_{kin} of 5–10 eV. The microstructure is less compact (Fig. 5d), resulting in a considerably higher electrical resistivity (455 μΩ cm, Fig. 6). On the other hand, the DC biased sample showed higher compressive stress (–5.2 GPa) and much lower electrical resistivity (40 μΩ cm, Fig. 6) due to a more compact structure (Fig. 5f). In a DC bias,

the potential is applied continuously, so not only Ti^+ ions are attracted to the substrate, but also Ar^+ ions, which are known to appear in the HiPIMS afterglow [23,73]. In the present case, we believe that the Ar^+ bombardment is the main reason behind the considerably higher compressive stress, in line with observations by Greczynski *et al.* [22,23] on TiAlN, since there are no reports of significant fluxes of ionized target material to the substrate during the afterglow. Note, however, that this mechanism is likely not dominating in the Moderate-energy series when using a DC bias during HiPIMS. For that series, the effect of impinging Ti^{2+} (and possibly higher charge states) onto the substrate are dominating and leading to very high compressive stress, as previously concluded.

The effect of ion bombardment on texture evolution in sputter-deposited TiN films has been largely discussed in the literature [45,46,47,49,59,61,74,75,76,77,78,79,80,81]. If thermodynamics plays a role in governing the early growth stages, favoring nucleation of (200) crystallites due to minimization of surface energy [45,74], recent reports have demonstrated the importance of growth kinetics and ion bombardment effects on the variation of preferred orientation and texture crossover from (200) to (111) with increasing film thickness [49,61,75,77,79]. Due to anisotropy in surface diffusivities and adatom potential energies [77], a competitive columnar growth occurs under low-temperature, low-ion-irradiation deposition conditions, favoring in this case a (111) texture [49,59]. The texture changes usually to (200) with increasing substrate temperature [79], ion energy [46,61], N_2 partial pressure [49,78,81], or ionization degree (ratio of ion-to-metal Γ_i/Γ_{Me} fluxes) [61,75,80]. For HiPIMS discharges, Ehiasarian *et al.* reported a change from (111) to (200) with increasing discharge current, i.e. with increasing $\Gamma_{Ti^+}/\Gamma_{Ti}$ and $\Gamma_{N^+}/\Gamma_{N_2}$ ratios [80]. It is also known that ion-surface interaction depends on crystal orientation, so that under intense ion bombardment, grains with more open channeling directions, such as (200) or (220), will eventually survive [46].

While the (200) texture observed for the Low-energy TiN films can be related to conditions of sufficient adatom mobility (T_s = 300 °C, $\Gamma_{Ti^+}/\Gamma_{Ti} > 1$), the predominant (111) orientation for

the Moderate-energy series, characterized by a high flux fraction of Ti^{2+} ions, has most likely contributed to strain energy minimization [74,76]. Due to elastic anisotropy, grains with (111) orientation are elastically more compliant and may also incorporate a larger concentration of point defects, as discussed previously.

Finally, please note that the effects of N^+ or N_2^+ bombardment during film growth were neglected in all previous discussions. It is known that N^+ and N_2^+ exhibit significant kinetic energies in the range of a few eV with a large energy tail [82]. However, we expect them to have a minor impact on the film stress due to the lower mass of N (14 amu) compared to Ar (39.9 amu) and Ti (47.9 amu), which limits the momentum transfer.

5. Conclusions

The results presented in this work show that the HiPIMS process conditions have a strong effect on TiN film stress developed during growth and on the final microstructure, where the HiPIMS discharge parameters as well as the substrate bias conditions need to be selected with great care. The use of standard HiPIMS discharges and biased substrates to enable energetic metal ion bombardment resulted in very dense and compact TiN films. However, they exhibited extremely high intrinsic compressive stress (–11 GPa). This is likely related to the high flux fraction of doubly-charged Ti ions reaching the substrate, where the ion density fraction $n_{Ti^{2+}}/n_{Ti^{+}}$ is known to increase with increasing peak current. Decreasing the pulse peak current density to around 0.2 A cm^{-2} resulted in a considerably reduced stress, reaching values in the order of –1 GPa. By furthermore adding synchronized pulsed substrate bias, the film properties could be fine-tuned in terms of mass density, surface roughness, and electrical resistivity, while still maintaining a low stress state. However, when using DC-biasing, the intrinsic stress was much more compressive, –5 GPa, due to a large fraction of Ar^+ ions that are accelerated by the bias potential during the HiPIMS afterglow.

Acknowledgements

The authors wish to acknowledge Dr. Philippe Guérin for his technical assistance on the sputter-deposition system. This work was supported by the French National Center for Scientific Research (CNRS) and the Brazilian National Council of Scientific and Technological Development (CNPq, "Ciência sem Fronteiras") through Project No. 233194/2014-2. FC is CNPq fellow. GA acknowledges financial support from the MC^2 project funded by French ANR program (Project No. ANR-13-MERA-0002-02). The authors are grateful to CTU IEF-Minerve, which is partly supported by the RENATECH network and the General Council of Essonne.

List of Figure and Table Captions

Figure 1. (a) Discharge voltage and current waveforms for the Low-energy HiPIMS process during TiN deposition. The different substrate bias voltage waveforms recorded during depositions are shown for (b) grounded and DC biased substrates and (c-e) pulsed biased substrates, synchronized with the HiPIMS pulse at different delay times (t_{bias}). The golden arrows signalize the time at which the bias pulse is turned on in respect to the HiPIMS discharge pulse, for each case investigated.

Figure 2. Evolution of the film force (F/w) and the average intrinsic stress with film thickness during deposition of TiN at different substrate conditions using (a,c) Moderate-energy and (b,d) Low-energy HiPIMS discharges. For the Moderate-energy case, a DCMS TiN sample is also presented (dashed line). The substrate bias voltage was –60 V for all biased samples (DC or pulsed). The pulsed biased samples are indicated by their different delay times (t) in respect to the HiPIMS discharge pulse. Selected average stress values are indicated in (c,d), which were recorded at specific film thicknesses.

Figure 3. Average intrinsic stress of TiN thin films as a function of the substrate condition (grounded, DC, or pulsed bias synchronized at different delay times (t) in respect to the HiPIMS

discharge pulse). The values indicated in the light-grey portion are referred to films deposited by HiPIMS, whereas the dark-grey portion accounts for a DCMS sample.

Figure 4. XRD patterns of the TiN films deposited by (a) Moderate-energy and (b) Low-energy HiPIMS at different substrate conditions. The bias voltage was –60 V for all biased samples. For the pulsed bias case, only the $t_{\mathrm{bias}} = 60$ µs condition is shown, since it does not differ from the $t_{\mathrm{bias}} = 1$ µs and 30 µs conditions. The film thickness of all samples shown in (a) is 200 nm, whereas it is 300–400 nm for the samples shown in (b).

Figure 5. Cross-sectional SEM images of the TiN films deposited by (a,b) Moderate-energy HiPIMS, (c) DCMS using equivalent conditions, and (d-f) Low-energy HiPIMS. The substrate condition is indicated for each sample. The bias voltage was –60 V for all biased samples. The delay time for the pulsed biased samples was 1 µs.

Figure 6. Electrical resistivity of TiN films deposited under Moderate- and Low-energy HiPIMS as a function of their intrinsic stresses. Labels near the symbols denote the bias conditions (g = grounded, dc = DC bias); symbols without a label correspond to pulsed bias. The DCMS sample is also included.

Table 1. TiN film properties for the Moderate-energy series (superscript "a") and the Low-energy series (superscript "b"), as measured by XRR, SEM, WDS, XRD and electrical resistivity. In columns "FWHM" and "T_c", the first and second values in each line are related to the 111 and the 200 reflections, respectively.

Growth condition	Mass density (g cm^{-3})	Surface roughness (nm)	Film thickness (nm)	N/Ti	O (at.%)	ρ_{el} (µΩ cm)	FWHM (°)	T_c
grounded	5.20 [a] 4.15 [b]	4.2 [a] 8.1 [b]	197 [a] 410 [b]	0.80 [a] 0.80 [b]	7.8 [a] 8.4 [b]	73 [a] 455 [b]	0.38/0.55[a] 0.26/0.30 [b]	1.59/0.41[a] 1.13/0.93 [b]
DC bias	5.50 [a] 5.10 [b]	1.5 [a] 3.0 [b]	175 [a] 277 [b]	0.80 [a] 0.85 [b]	2.3 [a] 3.0 [b]	31 [a] 40 [b]	0.63/0.91[a] 0.60/0.45[b]	1.57/0.43[a] 1.27/1.37[b]

Pulsed bias, t_{bias}= 1 us	-	-	201 [a] 370 [b]	0.80 [a]	2.9 [a]	33 [a] 129 [b]	0.27/0.31[b]	0.47/1.79[b]
Pulsed bias, t_{bias}= 30 us	5.40 [a] 4.80 [b]	1.3 [a] 6.7 [b]	192 [a]	0.80 [a] 0.80 [b]	3.0 [a] 5.5 [b]	32 [a] 94 [b]	0.36/0.30[b]	0.39/2.11[b]
Pulsed bias, t_{bias}= 60 us	5.40 [a] 4.90 [b]	1.2 [a] 6.0 [b]	-	-	-	28 [a] 86 [b]	0.58/0.95[a] 0.46/0.31 [b]	1.55/0.45[a] 0.46/1.96[b]
DCMS film	4.55 [a]	7.2 [a]	190 [a]	0.80 [a]	14.1 [a]	267 [a]	-	-

References

[1] J.T. Gudmundsson, N. Brenning, D. Lundin, U. Helmersson, High power impulse magnetron sputtering discharge, J. Vac. Sci. Technol. A 30 (2012) 030801. https://doi.org/10.1116/1.3691832

[2] D. Lundin, K. Sarakinos, An introduction to thin film processing using high-power impulse magnetron sputtering, J. Mater. Res. 27 (2012) 780. https://doi.org/10.1557/jmr.2012.8

[3] M. Samuelsson, D. Lundin, J. Jensen, M.A. Raadu, J.T. Gudmundsson, U. Helmersson, On the film density using high power impulse magnetron sputtering, Surf. Coat. Technol. 205 (2010) 591. https://doi.org/10.1016/j.surfcoat.2010.07.041

[4] M. Lattemann, U. Helmersson, J.E. Greene, Fully dense, non-faceted 111-textured high power impulse magnetron sputtering TiN films grown in the absence of substrate heating and bias, Thin Solid Films 518 (2010) 5978. https://doi.org/10.1016/j.tsf.2010.05.064

[5] A. Aijaz, Y.-X. Ji, J. Montero, G.A. Niklasson, C.G. Granqvist, T. Kubart, Low-temperature synthesis of thermochromic vanadium dioxide thin films by reactive high power impulse magnetron sputtering, Sol. Energy Mater. Sol. Cells 149 (2016) 137. https://doi.org/10.1016/j.solmat.2016.01.009

[6] F. Cemin, M. Tsukamoto, J. Keraudy, U. Helmersson, F. Alvarez, T. Minea, D. Lundin, Low-energy ion irradiation in HiPIMS to enable anatase TiO_2 selective growth, J. Phys. D Appl. Phys. 51 (2018) 235301. https://doi.org/10.1088/1361-6463/aac080

[7] G. Greczynski, J. Lu, J. Jensen, I. Petrov, J.E. Greene, S. Bolz, W. Kölker, Ch. Schiffers, O. Lemmer, L. Hultman, Strain-free, single-phase metastable $Ti_{0.38}Al_{0.62}N$ alloys with high hardness: Metal-ion energy vs. momentum effects during film growth by hybrid high-power pulsed/dc magnetron cosputtering, Thin Solid Films 556 (2014) 87. https://doi.org/10.1016/j.tsf.2014.01.017

[8] F. Cemin, D. Lundin, D. Cammilleri, T. Maroutian, P. Lecoeur, T. Minea, Low electrical resistivity in thin and ultrathin copper layers grown by high power impulse magnetron sputtering, J. Vac. Sci. Technol. A 34 (2016) 051506. https://doi.org/10.1116/1.4959555

[9] L. Jablonka, L. Riekehr, Z. Zhang, S.-L. Zhang, T. Kubart, Highly conductive ultrathin Co films by high-power impulse magnetron sputtering, Appl. Phys. Lett. 112 (2018) 043103. https://doi.org/10.1063/1.5011109

[10] A.P. Ehiasarian, J.G. Wen, I. Petrov, Interface microstructure engineering by high power impulse magnetron sputtering for the enhancement of adhesion, J. Appl. Phys. 101 (2007) 054301. https://doi.org/10.1063/1.2697052

[11] J. Alami, P.O.Å. Persson, D. Music, J.T. Gudmundsson, J. Bohlmark, U. Helmersson, Ion-assisted physical vapor deposition for enhanced film properties on nonflat surfaces, J. Vac. Sci. Technol. A 23 (2005) 278. https://doi.org/10.1116/1.1861049

[12] T. Shimizu, H. Komiya, T. Watanabe, Y. Teranishi, H. Nagasaka, K. Morikawa, M. Yang, HIPIMS deposition of TiAlN films on inner wall of micro-dies and its applicability in micro-sheet metal forming, Surf. Coat. Technol. 250 (2014) 44. https://doi.org/10.1016/j.surfcoat.2014.02.008

[13] F. Cemin, D. Lundin, C. Furgeaud, A. Michel, G. Amiard, T. Minea, G. Abadias, Epitaxial growth of Cu(001) thin films onto Si(001) using a single-step HiPIMS process, Sci. Rep. 7 (2017) 1655. http://dx.doi.org/10.1038/s41598-017-01755-8

[14] E. Wallin, T.I. Selinder, M. Elfwing, U. Helmersson, Synthesis of α-Al_2O_3 thin films using reactive high-power impulse magnetron sputtering, Europhys. Lett. 82 (2008) 36002. https://doi.org/10.1209/0295-5075/82/36002

[15] F.M. D'Heurle, J.M.E. Harper, Note on the origin of intrinsic stresses in films deposited via evaporation and sputtering, Thin Solid Films 171 (1989) 81. https://doi.org/10.1016/0040-6090(89)90035-7

[16] C.A. Davis, A simple model for the formation of compressive stress in thin films by ion bombardment, Thin Solid Films 226 (1993) 30. https://doi.org/10.1016/0040-6090(93)90201-Y

[17] G. Carter, Peening in ion-assisted thin-film deposition: a generalized model, J. Phys. D: Appl. Phys. 27 (1994) 1046. https://doi.org/10.1088/0022-3727/27/5/024

[18] M.M.M. Bilek, D.R. McKenzie, A comprehensive model of stress generation and relief processes in thin films deposited with energetic ions, Surf. Coat. Technol. 200 (2006) 4345. https://doi.org/10.1016/j.surfcoat.2005.02.161

[19] D. Magnfält, G. Abadias, K. Sarakinos, Atom insertion into grain boundaries and stress generation in physically vapor deposited films, Appl. Phys. Lett. 103 (2013) 051910. https://doi.org/10.1063/1.4817669

[20] P.Eh. Hovsepian, A.A. Sugumaran, Y. Purandare, D.A.L. Loch, A.P. Ehiasarian, Effect of the degree of high power impulse magnetron sputtering utilization on the structure and properties of TiN film, Thin Solid Films 562 (2014) 132. https://doi.org/10.1016/j.tsf.2014.04.002

[21] R. Machunze, A.P. Ehiasarian, F.D. Tichelaar, G.C.A.M. Janssen, Stress and texture in HIPIMS TiN thin films, Thin Solid Films 518 (2009) 1561. https://doi.org/10.1016/j.tsf.2009.09.069

[22] G. Greczynski, J. Lu, J. Jensen, I. Petrov, J.E. Greene, S. Bolz, W. Kölker, C. Schiffers, O. Lemmer, L. Hultman, Metal versus rare-gas ion irradiation during $Ti_{1-x}Al_xN$ film growth by hybrid high power pulsed magnetron/dc magnetron co-sputtering using synchronized pulsed substrate bias, J. Vac. Sci. Technol. A 30 (2012) 061504. https://doi.org/10.1116/1.4750485

[23] G. Greczynski, J. Lu, J. Jensen, S. Bolz, W. Kölker, Ch. Schiffers, O. Lemmer, J.E. Greene, L. Hultman, A review of metal-ion-flux-controlled growth of metastable TiAlN by HIPIMS/DCMS co-sputtering, Surf. Coat. Technol. 257 (2014) 15. https://doi.org/10.1016/j.surfcoat.2014.01.055

[24] A. Anders, J. Andersson, A. Ehiasarian, High power impulse magnetron sputtering: Current-voltage-time characteristics indicate the onset of sustained self-sputtering, J. Appl. Phys. 102 (2007) 113303. https://doi.org/10.1063/1.2817812

[25] C. Huo, D. Lundin, J.T. Gudmundsson, M.A. Raadu, J.W. Bradley, N. Brenning, Particle-balance models for pulsed sputtering magnetrons, J. Phys. D. Appl. Phys. 50 (2017) 354003. https://doi.org/10.1088/1361-6463/aa7d35

[26] G. Greczynski, I. Petrov, J.E. Greene, L. Hultman, Strategy for tuning the average charge state of metal ions incident at the growing film during HIPIMS deposition, Vacuum 116 (2015) 36. https://doi.org/10.1016/j.vacuum.2015.02.027

[27] S. Zhang, W. Zhu, TiN coating of tool steels: a review, J. Mater. Process. Technol. 39 (1993) 165. https://doi.org/10.1016/0924-0136(93)90016-Y

[28] H.O. Pierson. Handbook of refractory carbides and nitrides: properties, characteristics, processing, and applications. Westwood, NJ: Noyes Publications, 1996.

[29] A.E. Kaloyeros, E. Eisenbraun, Ultrathin Diffusion Barriers/Liners for Gigascale Copper Metallization, Annu. Rev. Mater. Sci. 30 (2000) 363. https://doi.org/10.1146/annurev.matsci.30.1.363

[30] S. Niyomsoan, W. Grant, D.L. Olson, B. Mishra, Variation of color in titanium and zirconium nitride decorative thin films, Thin Solid Films 415 (2002) 187. https://doi.org/10.1016/S0040-6090(02)00530-8

[31] W.-Y. Wu *et al.*, Bioapplication of TiN thin films deposited using high power impulse magnetron sputtering, Surf. Coat. Technol. 362 (2019) 167. https://doi.org/10.1016/j.surfcoat.2019.01.106

[32] P. Patsalas, N. Kalfagiannis, S. Kassavetis, Optical Properties and Plasmonic Performance of Titanium Nitride, Materials 8 (2015) 3128. https://doi.org/10.3390/ma8063128

[33] A. Lalisse, G. Tessier, J. Plain, G. Baffou, Plasmonic efficiencies of nanoparticles made of metal nitrides (TiN, ZrN) compared with gold, Sci. Rep. 6 (2016) 38647. https://doi.org/10.1038/srep38647

[34] U. Guler *et al.*, Local Heating with Lithographically Fabricated Plasmonic Titanium Nitride Nanoparticles, Nano Lett. 13 (2013) 6078. https://doi.org/10.1021/nl4033457

[35] G. Abadias *et al*, Review Article: Stress in thin films and coatings: Current status, challenges, and prospects, J. Vac. Sci. Technol. A 36 (2018) 020801. https://doi.org/10.1116/1.5011790

[36] A.E. Ross, R. Sangines, B. Treverrow, M.M.M. Bilek, D.R. McKenzie, Optimizing efficiency of Ti ionized deposition in HIPIMS, Plasma Sources Sci. Technol. 20 (2011) 035021. https://doi.org/10.1088/0963-0252/20/3/035021

[37] T. Kubart, M. Čada, D. Lundin, Z. Hubička, Investigation of ionized metal flux fraction in HiPIMS discharges with Ti and Ni targets, Surf. Coat. Technol. 238 (2014) 152. https://doi.org/10.1016/j.surfcoat.2013.10.064

[38] D. Lundin, M. Čada, Z. Hubička, Ionization of sputtered Ti, Al, and C coupled with plasma characterization in HiPIMS, Plasma Sources Sci. Technol. 24 (2015) 035018. https://doi.org/10.1088/0963-0252/24/3/035018

[39] B. Chapman. Glow discharge processes: sputtering and plasma etching. New York, NY: John Wiley and Sons, 1980.

[40] A. Fillon, G. Abadias, A. Michel, C. Jaouen, Stress and microstructure evolution during growth of magnetron-sputtered low-mobility metal films: Influence of the nucleation conditions, Thin Solid Films 519 (2010) 1655. https://doi.org/10.1016/j.tsf.2010.07.091

[41] E. Chason, P.R. Guduru, Tutorial: Understanding residual stress in polycrystalline thin films through real-time measurements and physical models, J. Appl. Phys. 119 (2016) 191101. https://doi.org/10.1063/1.4949263

[42] G.G. Stoney, The Tension of Metallic Films Deposited by Electrolysis, Proc. R. Soc. A 82 (1909) 172. http://doi.org/10.1098/rspa.1909.0021

[43] G.C.A.M. Janssen, M.M. Abdalla, F. van Keulen, B.R. Pujada, B. van Venrooy, Celebrating the 100th anniversary of the Stoney equation for film stress: Developments from polycrystalline steel strips to single crystal silicon wafers, Thin Solid Films 517 (2009) 1858. https://doi.org/10.1016/j.tsf.2008.07.014

[44] C.S. Barret, T.B. Massalski. Structure of Metals: Crystallographic Methods, Principles and Data. Oxford, UK: Pergamon Press, 1980.

[45] J. Pelleg, L.Z. Zevin, S. Lungo, N. Croitoru, Reactive-sputter-deposited TiN films on glass substrates, Thin Solid Films 197 (1991) 117. https://doi.org/10.1016/0040-6090(91)90225-M

[46] I. Petrov, L. Hultman, J.- E. Sundgren, J.E. Greene, Polycrystalline TiN films deposited by reactive bias magnetron sputtering: Effects of ion bombardment on resputtering rates, film composition, and microstructure, J. Vac. Sci. Technol. A 10 (1992) 265. https://doi.org/10.1116/1.578074

[47] G. Abadias, Stress and preferred orientation in nitride-based PVD coatings, Surf. Coat. Technol. 202 (2008) 2223. https://doi.org/10.1016/j.surfcoat.2007.08.029

[48] A.L. Patterson, The Scherrer Formula for X-Ray Particle Size Determination, Phys. Rev. 56 (1939) 978. https://doi.org/10.1103/PhysRev.56.978

[49] S. Mahieu, D. Depla, Reactive sputter deposition of TiN layers: modelling the growth by characterization of particle fluxes towards the substrate, J. Phys. D: Appl. Phys. 42 (2009) 053002. https://doi.org/10.1088/0022-3727/42/5/053002

[50] J.-E. Sundgren, Structure and properties of TiN coatings, Thin Solid Films 128 (1985) 21. https://doi.org/10.1016/0040-6090(85)90333-5

[51] B.W. Karr, D.G. Cahill, I. Petrov, J.E. Greene, Effects of high-flux low-energy ion bombardment on the low-temperature growth morphology of TiN(001) epitaxial layers, Phys. Rev. B 61 (2000) 16137. https://doi.org/10.1103/PhysRevB.61.16137

[52] B.-O. Johansson, J.-E. Sundgren, J.E. Greene, A. Rockett, S.A. Barnett, Growth and properties of single crystal TIN films deposited by reactive magnetron sputtering, J. Vac. Sci. Technol. A 3 (1985) 303. https://doi.org/10.1116/1.573255

[53] Y.P. Purandare, A.P. Ehiasarian, P.Eh. Hovsepian, Structure and properties of ZrN coatings deposited by high power impulse magnetron sputtering technology, J. Vac. Sci. Technol. A 29 (2011) 011004. https://doi.org/10.1116/1.3520640

[54] S.M. Deambrosis *et al.*, $Ti_{1-x}Al_xN$ coatings by Reactive High Power Impulse Magnetron Sputtering: film/substrate interface effect on residual stress and high temperature oxidation, Surf. Coat. Technol. 354 (2018) 56. https://doi.org/10.1016/j.surfcoat.2018.09.004

[55] J. Bohlmark, M. Lattemann, J.T. Gudmundsson, A.P. Ehiasarian, Y.A. Gonzalvo, N. Brenning, U. Helmersson, The ion energy distributions and ion flux composition from a high power impulse magnetron sputtering discharge, Thin Solid Films 515 (2006) 1522. https://doi.org/10.1016/j.tsf.2006.04.051

[56] D. Lundin, P. Larsson, E. Wallin, M. Lattemann, N. Brenning, U. Helmersson, Cross-field ion transport during high power impulse magnetron sputtering, Plasma Sources Sci. Technol. 17 (2008) 035021. https://doi.org/10.1088/0963-0252/17/3/035021

[57] F. Eriksson, N. Ghafoor, F. Schäfers, E.M. Gullikson, J. Birch, Interface engineering of short-period Ni/V multilayer X-ray mirrors, Thin Solid Films 500 (2006) 84. https://doi.org/10.1016/j.tsf.2005.11.019

[58] L. Wei, M. Zhong-Quan, W. Ye, W. De-Ming, Optimization of energy scope for titanium nitride films grown by ion beam-assisted deposition, Chin. Phys. Lett. 23 (2006) 178. https://doi.org/10.1088/0256-307X/23/1/052

[59] I. Petrov, P.B. Barna, L. Hultman, J.E. Greene, Microstructural evolution during film growth, J. Vac. Sci. Technol. A 21 (2003) S117. https://doi.org/10.1116/1.1601610

[60] I. Petrov, L. Hultman, U. Helmersson, J.-E. Sundgren, J.E. Greene, Microstructure modification of TiN by ion bombardment during reactive sputter deposition, Thin Solid Films 169 (1989) 299–314. https://doi.org/10.1016/0040-6090(89)90713-X

[61] P. Patsalas, C. Gravalidis, S. Logothetidis, Surface kinetics and subplantation phenomena affecting the texture, morphology, stress, and growth evolution of titanium nitride films, J. Appl. Phys. 96 (2004) 6234. https://doi.org/10.1063/1.1811389

[62] J. T. Gudmundsson, D. Lundin, N. Brenning, M. A. Raadu, C. Huo, T. M. Minea, An ionization region model of the reactive Ar/O_2 high power impulse magnetron sputtering discharge, Plasma Sources Sci. Technol. 25 (2016) 65004. https://doi.org/10.1088/0963-0252/25/6/065004

[63] P. Patsalas, C. Charitidis, S. Logothetidis, C.A. Dimitriadis, O. Valassiades, Combined electrical and mechanical properties of titanium nitride thin films as metallization materials, J. Appl. Phys. 86 (1999) 5296. https://doi.org/10.1063/1.371514

[64] C.-S. Shin, S. Rudenja, D. Gall, N. Hellgren, T.-Y. Lee, I. Petrov, J.E. Greene, Growth, surface morphology, and electrical resistivity of fully strained substoichiometric epitaxial TiNx ($0.67 \leqslant x < 1.0$) layers on MgO(001), J. Appl. Phys. 95 (2004) 356. https://doi.org/10.1063/1.1629155

[65] R. Koch, Stress in Evaporated and Sputtered Thin Films – A Comparison, Surf. Coat. Technol. 204 (2010) 1973. https://doi.org/10.1016/j.surfcoat.2009.09.047

[66] R.W. Hoffman, Stresses in thin films: The relevance of grain boundaries and impurities, Thin Solid Films 34 (1976) 185. https://doi.org/10.1016/0040-6090(76)90453-3

[67] I. Petrov, A. Myers, J.E. Greene, J.R. Abelson, Mass and energy resolved detection of ions and neutral sputtered species incident at the substrate during reactive magnetron sputtering of Ti

in mixed Ar+N_2 mixtures, J. Vac. Sci. Technol. A 12 (1994) 2846. https://doi.org/10.1116/1.578955

[68] C. Christou, Z.H. Barber, Ionization of sputtered material in a planar magnetron discharge, J. Vac. Sci. Technol. A 18 (2000) 2897. https://doi.org/10.1116/1.1312370

[69] S. Konstantinidis, A. Ricard, M. Ganciu, J.P. Dauchot, C. Ranea, M. Hecq, Measurement of ionic and neutral densities in amplified magnetron discharges by pulsed absorption spectroscopy, J. Appl. Phys. 95 (2004) 2900. https://doi.org/10.1063/1.1646452

[70] J.A. Thornton, D.W. Hoffman, Stress-related effects in thin films, Thin Solid Films 171 (1989) 5. https://doi.org/10.1016/0040-6090(89)90030-8

[71] H. Windischmann, Intrinsic stress in sputter-deposited thin films, Crit. Rev. Solid State Mater. Sci. 17 (1992) 547. https://doi.org/10.1080/10408439208244586

[72] A Hecimovic, A.P. Ehiasarian, Spatial and temporal evolution of ion energies in high power impulse magnetron sputtering plasma discharge, J. Appl. Phys. 108 (2010) 063301. https://doi.org/10.1063/1.3486018

[73] M. Aiempanakit, A. Aijaz, D. Lundin, U. Helmersson, T. Kubart, Understanding the discharge current behavior in reactive high power impulse magnetron sputtering of oxides, J. Appl. Phys. 113 (2013) 133302. https://doi.org/10.1063/1.4799199

[74] J.P. Zhao, X. Wang, Z.Y. Chen, S.Q. Yang, T.S. Shi, X.H. Liu, Overall energy model for preferred growth of TiN films during filtered arc deposition, J. Phys. D. Appl. Phys. 30 (1997) 5. https://doi.org/10.1088/0022-3727/30/1/002

[75] L. Hultman, J.- E. Sundgren, J.E. Greene, D.B. Bergstrom, I. Petrov, High- flux low-energy (≈20 eV) N^{2+} ion irradiation during TiN deposition by reactive magnetron sputtering:

Effects on microstructure and preferred orientation, J. Appl. Phys. 78 (1995) 5395. https://doi.org/10.1063/1.359720

[76] U.C. Oh, J.H. Je, Effects of strain energy on the preferred orientation of TiN thin films, J. Appl. Phys. 74 (1993) 1692. https://doi.org/10.1063/1.355297

[77] D. Gall, S. Kodambaka, M.A. Wall, I. Petrov, J.E. Greene, Pathways of atomistic processes on TiN(001) and (111) surfaces during film growth: An ab initio study, J. Appl. Phys. 93 (2003) 9086. https://doi.org/10.1063/1.1567797

[78] R. Banerjee, K. Singh, P. Ayyub, M.K. Totlani, A.K. Suri, Influence of the Ar/N2 ratio on the preferred orientation and optical reflectance of reactively sputter deposited titanium nitride thin films, J. Vac. Sci. Technol. A 21 (2003) 310. https://doi.org/10.1116/1.1531132

[79] G. Abadias, Y.Y. Tse, P. Guérin, V. Pelosin, Interdependence between stress, preferred orientation, and surface morphology of nanocrystalline TiN thin films deposited by dual ion beam sputtering, J. Appl. Phys. 99 (2006) 113519. https://doi.org/10.1063/1.2197287

[80] A.P. Ehiasarian, A. Vetushka, Y.A. Gonzalvo, G. Sfrn, L. Székely, P.B. Barna, Influence of high power impulse magnetron sputtering plasma ionization on the microstructure of TiN thin films, J. Appl. Phys. 109 (2011) 104314. https://doi.org/10.1063/1.3579443

[81] G. Abadias, W.P. Leroy, S. Mahieu, D. Depla, Influence of particle and energy flux on stress and texture development in magnetron sputtered TiN films, J. Phys. D. Appl. Phys. 46 (2013) 055301. https://doi.org/10.1088/0022-3727/46/5/055301

[82] P.-Y. Jouan, L. Le Brizoual, M. Ganciu, C. Cardinaud, S. Tricot, M.A. Djouadi, HiPIMS Ion Energy Distribution Measurements in Reactive Mode, IEEE Trans. Plasma Sci. 38 (2010) 3089. https://doi.org/10.1109/TPS.2010.2073688

Highlights

- Low stress TiN films are obtained by low-energy ion bombardment in HiPIMS.
- A new process window is found between standard HiPIMS and DCMS discharges.
- TiN film properties are fine-tuned using synchronized pulsed substrate bias.

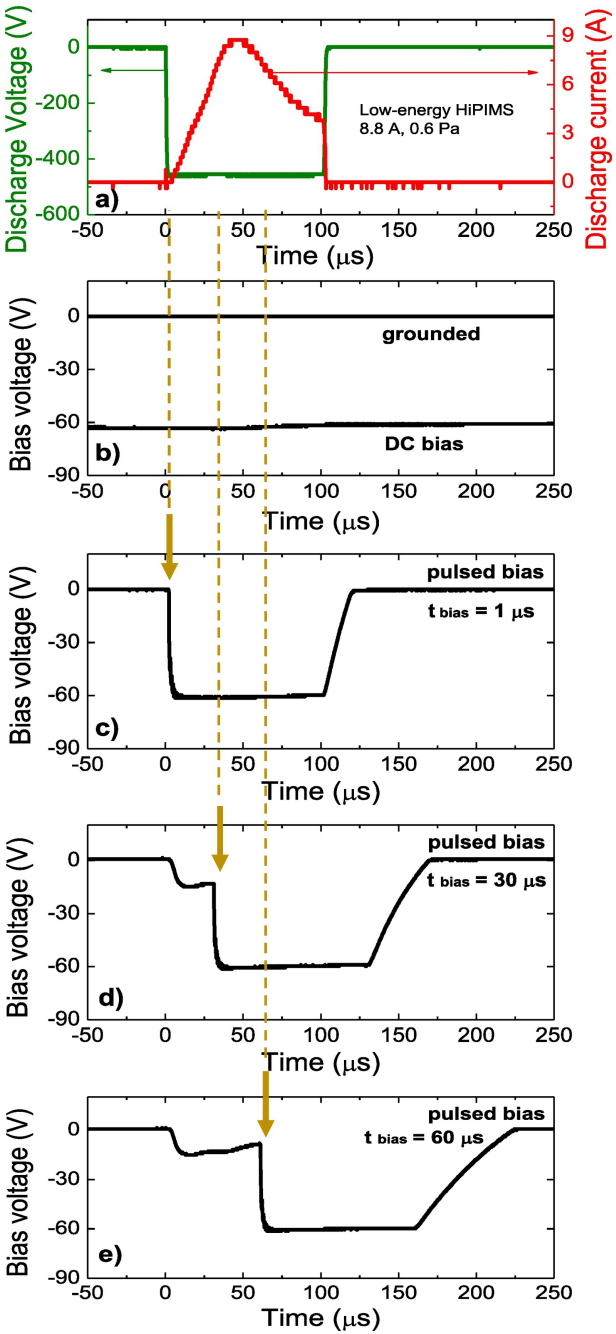
Discharge Voltage (V)
Discharge current (A)
Low-energy HiPIMS
8.8 A, 0.6 Pa
a)
Time (μs)
Bias voltage (V)
grounded
DC bias
b)
Time (μs)
pulsed bias
t bias = 1 μs
c)
Time (μs)
pulsed bias
t bias = 30 μs
d)
Time (μs)
pulsed bias
t bias = 60 μs
e)
Time (μs)

Figure 1

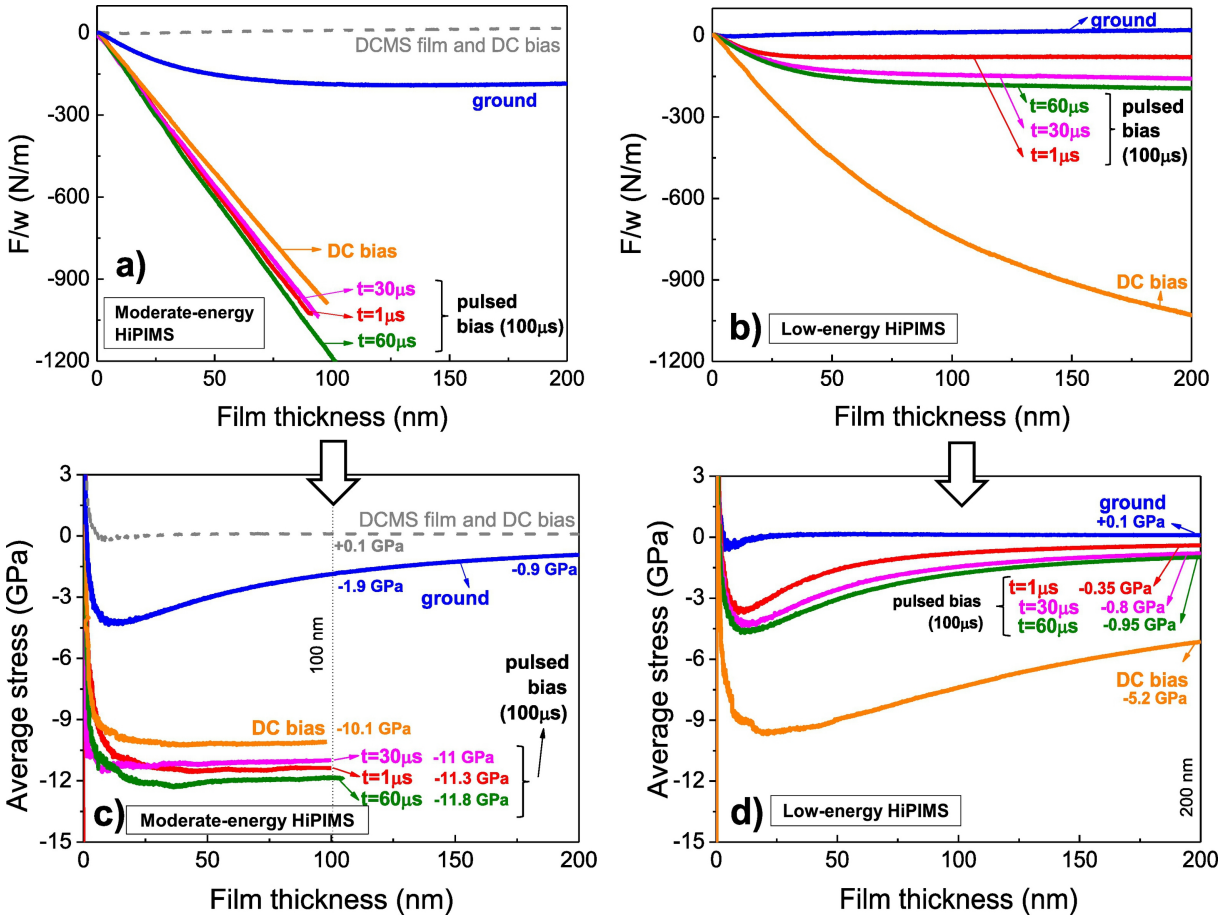
a)
Moderate-energy HiPIMS
DCMS film and DC bias
ground
DC bias
t=30μs
t=1μs
t=60μs
pulsed bias (100μs)
F/w (N/m)
Film thickness (nm)
b)
Low-energy HiPIMS
ground
t=60μs
t=30μs
t=1μs
pulsed bias (100μs)
DC bias
F/w (N/m)
Film thickness (nm)
c)
Moderate-energy HiPIMS
DCMS film and DC bias
+0.1 GPa
-0.9 GPa
-1.9 GPa
ground
100 nm
pulsed bias (100μs)
DC bias
-10.1 GPa
t=30μs -11 GPa
t=1μs -11.3 GPa
t=60μs -11.8 GPa
Average stress (GPa)
Film thickness (nm)
d)
Low-energy HiPIMS
ground
+0.1 GPa
pulsed bias (100μs)
t=1μs -0.35 GPa
t=30μs -0.8 GPa
t=60μs -0.95 GPa
DC bias
-5.2 GPa
200 nm
Average stress (GPa)
Film thickness (nm)

Figure 2

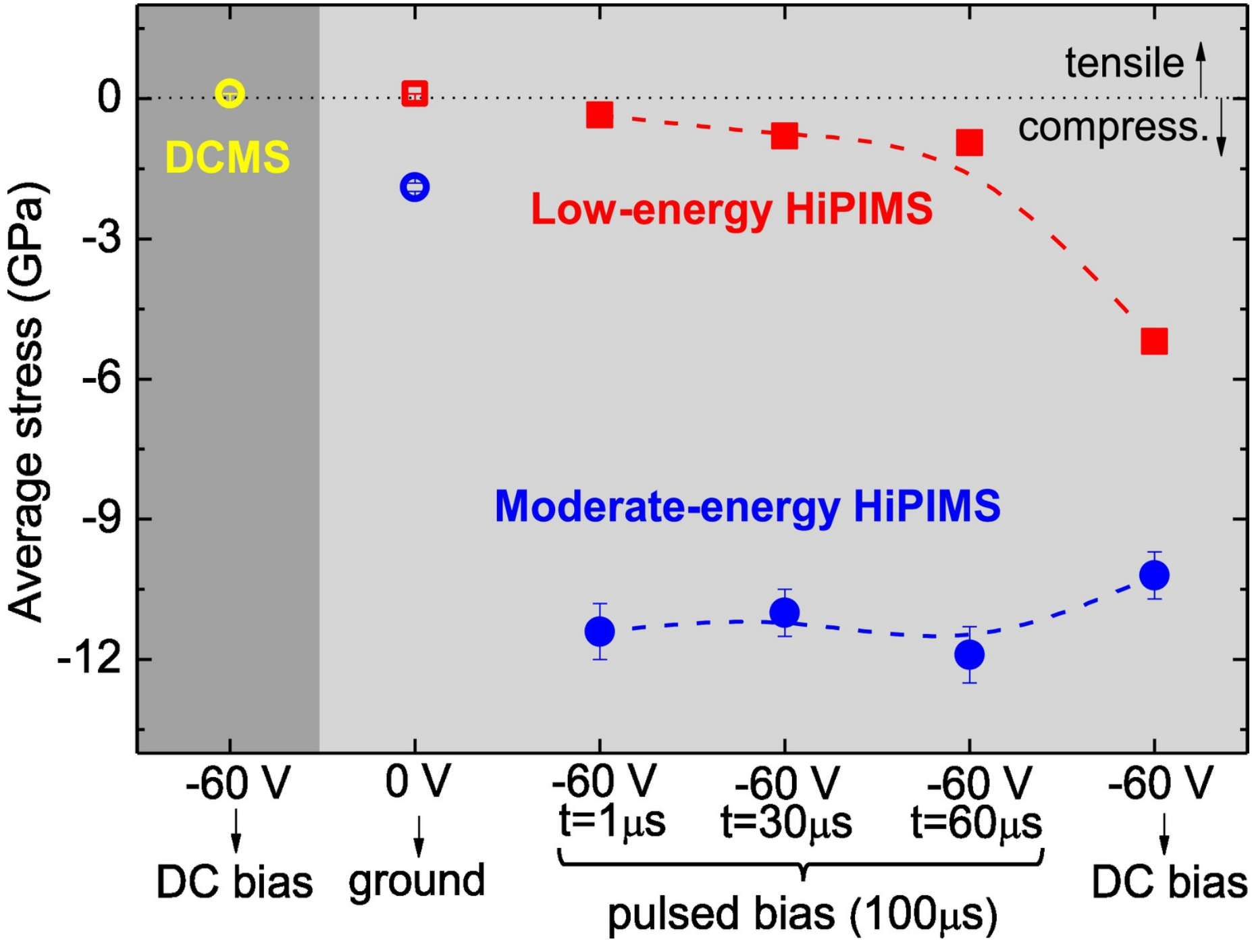
tensile
compress.
0
-3
-6
-9
-12
Average stress (GPa)
DCMS
Low-energy HiPIMS
Moderate-energy HiPIMS
-60 V
DC bias
0 V
ground
-60 V
t=1μs
-60 V
t=30μs
-60 V
t=60μs
pulsed bias (100μs)
-60 V
DC bias

Figure 3

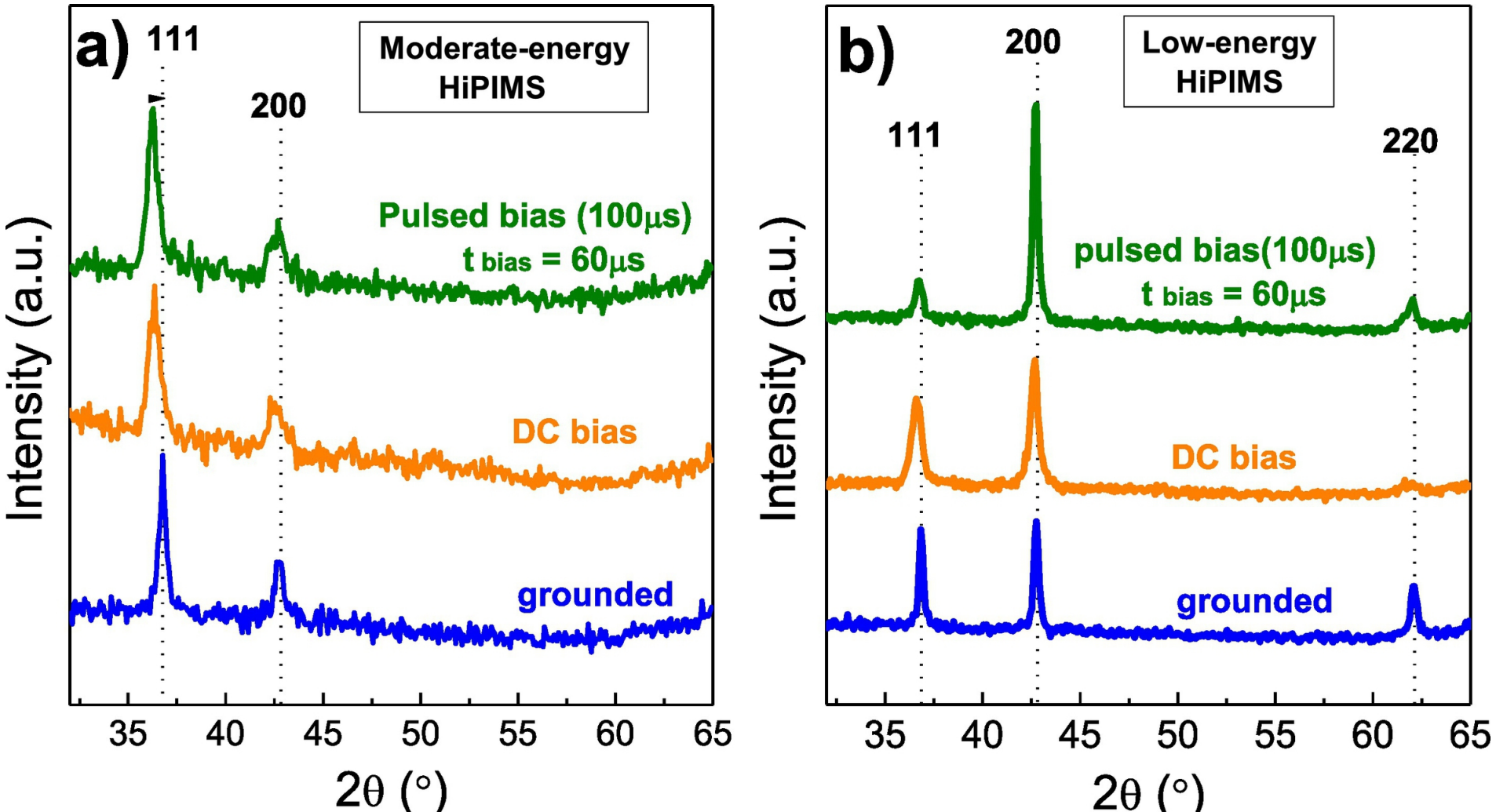
a)
111
200
Moderate-energy HiPIMS
Pulsed bias (100μs)
t bias = 60μs
DC bias
grounded
Intensity (a.u.)
35
40
45
50
55
60
65
2θ (°)
b)
200
111
220
Low-energy HiPIMS
pulsed bias(100μs)
t bias = 60μs
DC bias
grounded
Intensity (a.u.)
35
40
45
50
55
60
65
2θ (°)

Figure 4

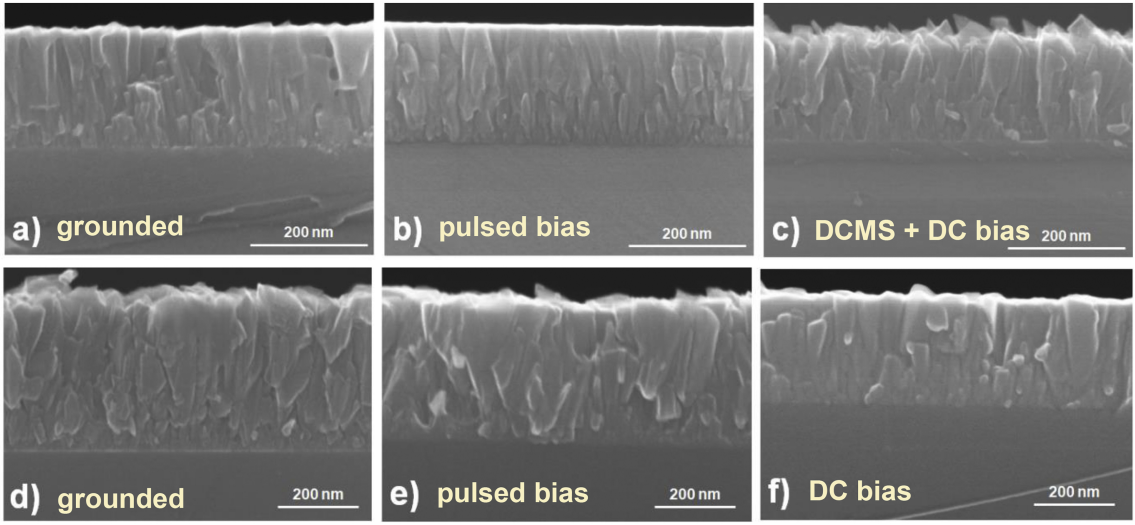
a) grounded
200 nm
b) pulsed bias
200 nm
c) DCMS + DC bias
200 nm
d) grounded
200 nm
e) pulsed bias
200 nm
f) DC bias
200 nm

Figure 5